Contents lists available at ScienceDirect

Neurochemistry International

journal homepage: http://ees.elsevier.com

Detection and quantification of the anti-obesity drug celastrol in murine liver and brain

Meri De Angelis [a,*], Sonja C. Schriever [b,c,d], Eleni Kyriakou [e,f], Michael Sattler [e,f], Ana C. Messias [e,f], Karl-Werner Schramm [a,g], Paul T. Pfluger [b,c,d,h,**]

[a] Helmholtz Zentrum München-German Research Center for Environmental Health (GmbH), Molecular EXposomics, Ingolstädter Landstr. 1, 85764, Neuherberg, Germany
[b] Helmholtz Zentrum München-German Research Center for Environmental Health (GmbH), Research Unit Neurobiology of Diabetes, 85764, Neuherberg, Germany
[c] Helmholtz Zentrum München-German Research Center for Environmental Health (GmbH) Institute for Diabetes and Obesity, 85764, Neuherberg, Germany
[d] German Center for Diabetes Research (DZD), 85764, Neuherberg, Germany
[e] Helmholtz Zentrum München-German Research Center for Environmental Health (GmbH), Institute of Structural Biology, 85764, Neuherberg, Germany
[f] Technical University of Munich, Biomolecular NMR and Center for Integrated Protein Science Munich at Department of Chemistry, 85747, Garching, Germany
[g] Technical University of Munich, Department für Biowissenschaftliche Grundlagen, 85350, Freising, Germany
[h] Technical University of Munich, Neurobiology of Diabetes, TUM School of Medicine, 81675, Munich, Germany

ARTICLE INFO

Keywords
Celastrol
Brain
Hypothalamus
Obesity
LC-MS
Leptin sensitizer

ABSTRACT

Celastrol is a natural pentacyclic triterpene extracted from the roots of *Tripterygium wilfordi* (thunder god vine). Celastrol was reported as a powerful anti-obese drug with leptin sensitizing properties that decreases food consumption and mediates body weight loss when administered to diet-induced obese mice at 100 μg/kg body weight. The weight lowering properties of celastrol are likely mediated by the CNS, in particular, by the hypothalamus, but the final proof for the accumulation of celastrol in the brain and hypothalamus remains to be established. Here, we aimed to demonstrate that intraperitoneal celastrol administration at 100 μg/kg can rapidly reach the brain and, in particular, the hypothalamus of mice. We developed and validated a sensitive liquid chromatography mass spectrometry method for the quantitative determination of celastrol in murine tissues, namely liver, brain and hypothalamus. Chow-fed lean mice were randomly assigned to the vehicle vs. celastrol groups, injected with saline or 100 μg/kg body weight of celastrol, and sacrificed 30 min or 120 min post injection. Celastrol was extracted from homogenized tissue using ethyl acetate as organic solvent, and quantified using a matrix-matched calibration curve with glycyrrhetinic acid as internal standard. Liver celastrol concentrations were 32.60 ± 8.21 pg/mg and 40.52 ± 15.6 pg/mg, 30 and 120 min after injection, respectively. We found 4.70 ± 0.31 pg/mg celastrol after 30 min, and 16.22 ± 3.33 pg/mg after 120 min in whole brain lysates, and detectable amounts in the hypothalamus. These results corroborate the validity of our methodology, demonstrate the accumulation of celastrol in the brain of mice injected intraperitoneally with a dose of 100 μg/kg, and confirm the CNS as possible site of action for the weight lowering properties of celastrol.

1. Introduction

Obesity is a health problem of the first order (Bluher, 2019; James, 2018) caused by an increasingly sedentary lifestyle and exacerbated food-consumption. Obesity is linked not only to metabolic disturbances, but also to behavioral alterations such as sleep (Hakim et al., 2015) or mood disorders (McElroy et al., 2004; Simon et al.), and perturbed sexual behavior (Bajos et al., 2010; Gordon et al., 2016). Obesity has further been associated with neuronal injuries in the human cerebellum and hippocampus (Mueller et al., 2012) and is, thus, considered a neurobiological disease (Kelestimur et al., 2017). Accordingly, anti-obesity drugs are warranted that elicit some of their action in CNS centers regulating body weight.

Celastrol (Fig. 1A) is a natural compound extracted from the root of the plant *Tripterygium wilfordi* that was shown to have anti-cancer (Kannaiyan et al., 2011; Kashyap et al., 2018), anti-oxidant (Allison et al., 2000, 2001), and anti-inflammatory (Allison et al., 2001; Kim et al., 2009) activities. Recent evidence further describes

* Corresponding author. Molecular EXposomics, Helmholtz Zentrum München-German Research Center for Environmental Health (GmbH), Ingolstädter Landstr. 1, 85764, Neuherberg, Germany.
** Corresponding author. Research Unit NeuroBiology of Diabetes, Helmholtz Zentrum München-German Research Center for Environmental Health (GmbH), Ingolstädter Landstr. 1, 85764, Neuherberg, Germany.
E-mail addresses: meri.deangelis@helmholtz-muenchen.de (M. De Angelis); paul.pfluger@helmholtz-muenchen.de (P.T. Pfluger)

https://doi.org/10.1016/j.neuint.2020.104713
Received 9 December 2019; Received in revised form 25 Febraury 2020; Accepted 3 March 2020
Available online xxx
0197-0186/© 2020.

UNCORRECTED PROOF

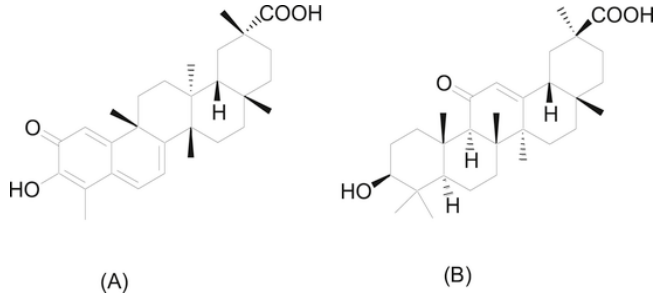

Fig. 1. Chemical structure of celastrol (A) and glycyrrhetinic acid (Internal standard (IS), B).

celastrol as a novel anti-obesity drug that mediates weight loss by acting as a leptin sensitizer (Liu et al., 2015) (Pfuhlmann et al., 2018). Several mechanisms have been proposed for celastrol's weight-lowering properties, but the exact pathway(s) are still not completely understood. Celastrol was shown to impair adipocyte differentiation and increase lipolysis *in vitro* in 3T3-L1 adipocyte cells (Choi et al., 2016). Celastrol further increased GLUT4-mediated glucose uptake in white adipose tissue and skeletal muscle (Fang et al., 2019) and the expression of hepatic Sirt1 (Zhang et al., 2017) in mice. Celastrol was moreover reported as inhibitor of proteasome activity (Wang et al., 2018) and as activator of a heat-shock response (Trott et al., 2008; Wang et al., 2018), potentially driven via a HSF1-PGC-1α transcriptional axis that was also linked with increased muscle and brown-adipose tissue (BAT) thermogenesis and inguinal white adipose tissue (iWAT) browning (Ma et al., 2015). We recently confirmed this impact of celastrol on BAT and iWAT browning, i.e. an increase in uncoupling protein 1 (UCP1) levels, but found comparable weight lowering efficacies of celastrol in both WT and UCP1 KO mice (Pfuhlmann et al., 2018). Rather than thermogenesis, our data suggested decreased food intake as key driver for the weight loss induced by celastrol. Potential mechanisms for this decreased food consumption in response to celastrol administration are the decreased expression of the hypothalamic neuropeptide galanin and its receptor (Fang et al., 2019), or an increased expression of interleukin 1 receptor 1 (IL1R1) (Feng et al., 2019). The latter report shows that IL1R1 knock-out mice exposed to celastrol exhibit no leptin-sensitizing or anti-obesity effect, suggesting that celastrol exhibits its anti-obesity effects via a pro-inflammatory signaling cascade (Feng et al., 2019). We recently showed that celastrol-induced weight loss is largely mediated by the inhibition of leptin negative regulators protein tyrosine phosphatase 1B (PTP1B) and T-cell PTP (TCPTP) in the arcuate nucleus of the hypothalamus (Kyriakou et al., 2018). Overall, these studies suggest a wide pharmacological range of celastrol action and multiple targets, but a prominent role for the CNS and especially the hypothalamus in mediating the weight lowering and leptin sensitizing effects of celastrol.

In order to induce changes within the CNS, celastrol must cross the brain barriers to reach its, putatively neuronal, target cells. Although, according to the literature, celastrol can reach the brain, its accumulation in specific brain regions (i.e. hypothalamus) has not been firmly established. At current, most reports focus on the quantification of celastrol in human or animal serum and plasma (Wang et al., 2008; Xu et al., 2007; Yan et al., 2017; Zhang et al., 2012). Only two papers report on the detection of celastrol in rodent brains. Gou et al., measured celastrol in rat brain after injection of 1 mg per kg body weight (BW) (Guo et al., 2017), while Huang et al. detected celastrol in mouse brains after the administration of 4 mg celastrol per kg BW (Huang et al., 2012). The doses applied differed substantially to the dose of 100 μg/kg BW that was required to induce weight loss and leptin re-sensitization in diet-induced obese (DIO) mice (Kyriakou et al., 2018; Liu et al., 2015; Pfuhlmann et al., 2018). Here, we describe the development and validation of a sensitive liquid chromatography mass spectrometry (LC-MS) method for the quantitative determination of low-dose celastrol in murine tissues, including the liver, brain and hypothalamus. With our methodology, we could successfully detect celastrol accumulation in the brain and hypothalamus 30 and 120 min after the injection of 100 μg celastrol per kg BW, with brain celastrol levels being 4- to 10-fold lower compared to the liver. These results contribute to enhance our understanding on celastrol as an emerging anti-obese drug that has rich pharmacological properties and a likely CNS action on feeding circuits.

2. Material and methods

2.1. Chemicals and reagents

Celastrol and glycyrrhetinic acid (internal standard) were purchased from Sigma-Aldrich (St. Louis, MO, USA). All other reagents and solvents were of ACS grade or LC-MS grade. Distilled water was obtained using a water distillation purification system and was used for the preparation of all aqueous solutions.

2.2. Preparation of standard and quality control samples

The stock solutions of celastrol and glycyrrhetinic acid were prepared in methanol at concentrations of 1 ng/μL and 200 pg/μL respectively. The solutions were stored at −20 °C in the dark. The stock solutions were further diluted in CH_3CN:H_2O (7:3) to obtain the working standard solutions. The calibration curve was obtained by spiking known amounts of working standard solutions to 200 μL blank tissue extract, respectively. The spiking amount of celastrol was 0.5 pg/μL, 1 pg/μL, 5 pg/μL, 10 pg/μL, 50 pg/μL, and 100 pg/μL respectively wherein the internal standard concentration was always 20 pg/μL. These sequences of spiked solution into tissue extract were considered as matrix-matched calibration standard. The quality control samples were prepared at low (5 pg/μL) and high concentration (50 pg/μL) in the same way as the tissue samples for analysis and were stored at −80 °C until analysis. Quality control samples were prepared from both murine liver and brain.

2.3. Instrumentation

Quantification of celastrol was performed using an Agilent 6470 triple quadrupole tandem mass spectrometry (LC-MS/MS) system coupled with Agilent 1290 Infinity II LC system. The flow rate was 0.3 mL/min, the column temperature was 40 °C and injection volumes were 20 μL. The mobile phases of the gradient HPLC method were water (A) and acetonitrile (B), each containing 0.1% formic acid (v/v). The following gradient program was adopted: 50% B kept for 2 min, ramped linearly to 70% B in 2 min, kept in this condition for 4 min, followed by an increase to 100% B in 1 min and held for 1 min to remove lipophilic components, finally returned to initial conditions in 0.2 min. Further 4.8 min were allowed for re-equilibration before the next injection. Celastrol and glycyrrhetinic acid were separated on a Zorbax Eclipse Plus C18 column (2.1 × 50 mm, 1.8 μm). Analytes were detected using an electrospray ionization source (ESI) interfaced in the positive ion mode. The tandem mass spectrometer was operated under multiple reaction monitoring mode (MRM). The MS/MS transitions (*m/z*), the fragmentation voltage (FV), the collision energy (CE), the cell accelerator voltage (CAV) and the dwell time for the analytes are reported in Table 1. The mass spectrometric parameters were set as follow: gas temperature 125 °C; gas flow 6 L per min; nebulizer pressure 55 psi; capillary voltage 5500V.

UNCORRECTED PROOF

Table 1
Optimized MS/MS parameters for the celastrol analysis.

compound	Q1 (*m/z*) [a]	Q3 (*m/z*) [a]	F (V) [c]	CE (V) [c]	CAV (V) [c]	Dwell (msec) [c]
Celastrol	451.3	201.1 (q) [b]	172	12	2	500
		215.1 (c) [b]	172	12	2	500
Glycyrrhetinic acid (I.S.)	471.4	317.4	174	50	1	500

[a] Ion-transitions are given as m/z for parent ion (Q1) and product ions (Q3).
[b] The first product ion is used for the quantification (q), the second for the confirmation (c).
[c] Compound optimized values for fragmentor (F), collision energy (CE), collision acceleration voltage (CAV) and dwell time.

2.4. Celastrol administration and tissue collection

Female C57BL/6J mice were obtained from Janvier Lab (Saint-Berthevin Cedex, France) and maintained on a 12-h dark-light cycle and had free access to diet and water. Mice were fed normal rodent chow (Altromin, #1314). Celastrol (BOC Science, Shirley, NY, USA, #34157-83-0) was dissolved in pure DMSO and diluted with PBS to a final concentration of 0.02 mg/mL in 1% DMSO for injections. 100 μg/kg BW of celastrol or PBS with 1% DMSO as vehicle was injected intraperitoneally (ip) in similar volume. Mice were injected with celastrol or vehicle over 3 consecutive days. Daily injections took place 2 h before dark onset. After the 3rd injection, mice were sacrificed by cervical dislocation 30 min or 120 min after injection. The livers were removed rapidly from the peritoneum, flash-frozen in liquid nitrogen and then transferred to −80 °C for storage. The brains were carefully dissected from the skull using small forceps and flash-frozen in liquid nitrogen. Brains were furthermore transferred to a flat glass surface on ice, and the hypothalamus was dissected from the surrounding brain areas using razor blades and coordinates of the Allen brain atlas (https://mouse.brain-map.org/static/atlas). All studies were approved by the State of Bavaria, Germany, and were performed without blinding the investigators.

2.5. Sample preparation

Samples were pestled at −200 °C to obtain a powder from which 50 mg of liver or 200 mg of brain were used for the extraction of celastrol. The 50 mg-tissue samples were homogenized in 200 μL of pure cold water by ultrasonication (Bandelin Electronics, Berlin, Germany) in an ice-cooling bath. To this mixture, 100 μL of internal standard (20 pg/μL) were added, the tube was then vortexed for 1 min and 4 mL of ethyl acetate were added. After 20 min of vortexing at room temperature and centrifugation (Multifuge 3S/3S-R, Thermo Scientific, Walthmann, USA) at 3500 g for 10 min, the supernatant was collected and the extraction procedure repeated one more time using 2 mL ethyl acetate and 2 min of vortexing. The pooled organic phase was evaporated to dryness under nitrogen stream and then reconstituted in 100 μL of CH_3CN:H_2O (7:3). This mixture was centrifuged at 3500 g for 10 min and the supernatant collected (about 80 μL) for injection into the LC-MS/MS system. The extraction of celastrol from 200 mg of brain tissue was performed accordingly, but with adapted volumes. I.e., the samples were homogenized using 400 μL of pure water and then extracted using 9 mL ethyl acetate. For the extraction of celastrol from the hypothalamus, the homogenization was performed with 100 μL of pure water and the extraction with 2 mL ethyl acetate.

2.6. Statistical analysis

All data are expressed as mean ± SD. Data acquisition, linearity of the standard curve and quantification of the samples were performed using Agilent MassHunter Workstation software. All the other data were generated using SigmaPlot (version 12.0).

3. Results and discussion

3.1 Method development

For the quantification of celastrol, three different molecules were tested as a possible internal standard (IS). The first was pristimerin, a close analogue to celastrol. However, this compound was too lipophilic and required high content of organic solvent for its elution. Next, we tested hederagenin and glycyrrhetinic acid. Glycyrrhetinic acid showed a retention time closer to that of celastrol and a higher signal intensity, and was thus chosen as internal standard (Fig. 1B).

For the detection of celastrol and its internal standard a UPLC-system coupled with triple-quadrupole (QQQ) mass detector using an electrospray ionization source in positive mode was used.

Sample preparation was based on previous reports that employed the extraction of celastrol from biological samples with an organic solvent, subsequent evaporation of the supernatant to dryness, and the reconstitution of the residue in the mobile phase for the analysis (Guo et al., 2017; Huang et al., 2012; Wang et al., 2008, 2019; Xu et al., 2007; Yan et al., 2017; Zhang et al., 2012). However, the extraction of celastrol from biological samples involves particular challenges due to its low solubility and chemical reactivity. Specifically, celastrol can perform Michael-addition with nucleophilic thiol-groups (Sreeramulu et al., 2009). This behavior makes the full extraction and recovery of celastrol from biological samples difficult, and could explain the relatively low recovery values of 51%–65% for celastrol spiked in rat plasma as reported by Zhang *et al.* and Wang et al. (Wang et al., 2008; Zhang et al., 2012). A more recent report observed that the extraction of celastrol from tissue using a simple liquid-liquid extraction protocol is even more complicated than that from plasma (Guo et al., 2017). We tried different approaches to increase this extraction efficacy from tissues, and tested various solvents (methanol, acetonitrile, chloroform, ethyl acetate, diethyl ether), pH values (neutral and acid), extraction times (from 5 min to 1h) and finally additionally solid-phase extraction methodologies (anion exchange resin, reverse phase cartridge). Unfortunately, these attempts were largely futile. We were unable to achieve good recovery values, but some conclusions can be drawn from our attempts. In general, celastrol recoveries were lower when solvents miscible with water (i.e. methanol or acetonitrile) were used instead of solvents with distinct phase separation. Both in methanol and acetonitrile we observed a detrimental loss of the celastrol signal intensity (over 90%) compared to the value in neat solvent. Notably, the procedure in methanol was very simple since tissue was homogenized directly in methanol, the solvent evaporated and the compound reconstituted in the HPLC solvent for analysis. Accordingly, we do not know whether the loss of celastrol signal intensity is due to a detrimental matrix effect or the presence of polar molecules that react with celastrol. Using less polar organic solvents reduced this interference. Among those solvents tested for the capability to extract celastrol from pure water, ethyl acetate and chloroform were the most effective with comparable recovery rates (>70%). Subsequently, we chose ethyl acetate as solvent for the extraction from real sample due to the reportedly good stability of celastrol in this solvent even at room temperature (Camelio et al., 2015). When this solvent was tested on a biological sample the signal intensity of the celastrol was three times higher compared to the results obtained with methanol. We further tested whether the addition of 0.1% formic to ethyl acetate can increase celastrol re-

UNCORRECTED PROOF

covery rates based on earlier reports that showed diminished covalent bond formation between the thiol group and celastrol after the addition of formic acid (Peng et al., 2010). However, we did not find any improvements in the recovery. Both too long and too short extraction procedures decreased the celastrol recovery rates, with best results being obtained for an extraction period of 20–30 min. For the solid-phase extraction approach, Bond Elut Plexa (PAX, 60 mg, 3 mL) and Bond Elut C18 resins (100 mg, 3 mL) were tested. Both cartridges were used according to the specification of the vendor. These experiments were initially performed using pure celastrol dissolved in neat solvent. Good results were achieved with the reverse phase resin (over 90% recovery), while with the anion exchange resin less than 5% of celastrol was recovered after the elution We next used C18 cartridges to extract celastrol from a biological sample, however the recovery was not better than that obtained with simple liquid-liquid extraction in ethyl acetate. Specifically for the liquid-liquid extraction, we had a maximum extraction efficacy of about 34.8%, calculated by comparing the peak area of the celastrol in spiked samples before ($n = 3$) and after ($n = 3$) extraction. The spiked samples had a celastrol concentration of 50 pg/μL and were generated using about 50 mg of mouse liver. To overcome the problem of the low recovery, a matrix-matched calibration curve was adopted that gave consistent and reproducible results despite low extraction efficacies. The same approach was reported by Wang et al., albeit at a higher recovery rate for celastrol of 65% (Wang et al., 2008).

3.2. Method validation

Calibration curves for celastrol were obtained by spiking 200 μL of tissue extract with standard solutions (100 μL) in the concentration of 0.5 pg/μL, 1 pg/μL, 5 pg/μL, 10 pg/μL, 50 pg/μL, and 100 pg/μL. The internal standard concentration was kept at 20 pg/μL. A correlation coefficient (r^2) of above 0.99 was obtained. The LOQ, calculated as signal/noise ratio >10, was 0.5 pg/μL. The matrix-matched calibration curve was built using liver tissue extract, and was suitable for the quantification of celastrol in brain and liver samples. The methodology was validated using 50 mg of tissue (brain and liver). However, when brain samples from treated animals were tested the results were in the lower part of the calibration curve. The analysis was thus repeated using 200 mg of brain tissue and a new matrix-matched calibration curve was built using 200 mg of liver extract. The goodness of the calibration was validated via spike recovery experiments at low and high concentrations using the same quantity of brain extract (supplementary material, Table S1). In two independent mouse brain and three independent mouse liver samples, no interference was observed in the representative chromatograms of the blank samples at the retention time of the analyte and internal standard (Fig. 2, and Fig. S1).

Before sample analysis, QC samples spiked either with 5 pg/μL or 50 pg/μL were prepared to test the goodness of the calibration curve. The analyte identification was based on the retention times compared with quantification standards and m/z ratios of the selected ions. Instrumental quality control was performed regularly by injecting blank solvents or standard solutions.

The intra-day precision and accuracy of the method were assessed by preparing and measuring three different quality control samples (QC) on a single day. The inter-day precision and accuracy, were tested by measuring four different batches prepared in four different days. Every batch was constituted of three QC samples (except in one case where only two samples were prepared). The quality control samples were prepared by spiking celastrol at two different concentrations (5 and 50 pg/μL) into either brain or liver extracts. The results reported for the brain (Table 2) and liver (Table S2, supplementary material) show a relative standard deviation (RSD %) less than 23% and an accuracy between 84 and 106%, For the precision, a relative standard deviation < 20% is considered acceptable. The accuracy should be within a range of 80–120%. In our case, the intra-day precision for the liver was about 23%. This value, although slightly outside the range, is nonetheless considered acceptable as the inter-day value was within range.

Next, we assessed the short- and long-term stability of celastrol in the prepared QC samples. We first found that celastrol remains stable when samples are kept in the autosampler at 10 °C for 6h in the dark. The mid-term (−20 °C after 3 days) and long-term (−80 °C for two weeks) stability of celastrol in the spiked samples was also investigated. The stability test was performed with three different samples prepared from liver and brain tissues spiked with 5 and 50 pg/μL celastrol standard solution. Celastrol levels remained stable in the liver samples but diminished in all brain samples for both the low and high concentration, indicating decomposition and a detrimental interaction with brain matrix components upon prolonged storage (Table 3, Table S3, supplementary material). Pure celastrol dissolved in neat solvent (CH_3CN:H_2O, 7:3) and kept for 2h at room temperature (the time necessary for the sample preparation) remained stable. For such experiment two different standard solutions (5 pg/μL and 50 pg/μL) were measured in triplicate. Both precision and accuracy were in the expected range, indicating that no decomposition at the conditions used in this or our preceding studies (Pfuhlmann et al., 2018) occurred.

3.3. Quantification of celastrol

After establishing and validating our novel and highly sensitive method, we next aimed to quantify the accumulation of celastrol in murine brain and liver tissues after a single low dose injection. Eleven mice were randomly assigned to control (n = 3) and test (n = 8) groups. The test group was injected i.p. with 100 μg/kg BW of celastrol and the animals sacrificed 30 or 120 min post injection.

We first assessed the concentration of celastrol in the liver, and found comparable levels of 32.6 and 40.52 pg/mg tissue 30 and 120min after the administration, respectively, indicating no significant hepatic accumulation between the time points (Table 4). A recent biodistribution study conducted with 1 mg celastrol per kg BW in rats reported hepatic accumulation of celastrol with levels reaching up to 4 μg/mL (8 μg/g) after 5 min post injection (Guo et al., 2017). Notably, in this study the administration of 1 or 3 mg celastrol per kg BW in rat led to a profound and dose dependent histological damage in the liver (Guo et al., 2017). Hepatotoxic effects of celastrol when administered at mg/kg doses have indeed raised considerable doubt on its clinical safety, and initiated intense efforts to identify non-toxic analogues (Hou et al., 2020). Our data nonetheless suggest that celastrol administered at low doses of 100 μg/kg may not accumulate to hepatic levels that cause major hepatotoxicity. However, that safety aspect for low dose celastrol requires specific testing.

Effects of celastrol on food intake and weight loss are likely driven by the CNS. Accordingly, we next aimed to quantify celastrol in the CNS and the hypothalamus of mice. As summarized in Table 4, we found substantial amounts of celastrol in the brain, with a 4-fold accumulation from 30 to 120 min post-injection. These values, despite the low number of animals, are in agreement with an earlier report that showed a 2- to 4-fold increase in the levels of mouse brain celastrol after administration of free celastrol or celastrol encapsulated in liposomes (4 mg/kg, respectively), respectively (Huang et al., 2012). We next assessed whether celastrol could be detected also in the hypothalamus, a brain region involved in the weight lowering action of celastrol. Initially, we used hypothalamus tissue from one animal sacrificed after 120 min post injection, but failed to quantify celastrol due to the low amount of tissue. We thus pooled two hypothalami and repeated the analysis using a total 27.5 mg hypothalamus tissue mass. Prior to the actual analysis of the celastrol-treated mouse hypothalami, we conducted a blank analysis of two hypothalamus samples from untreated

UNCORRECTED PROOF

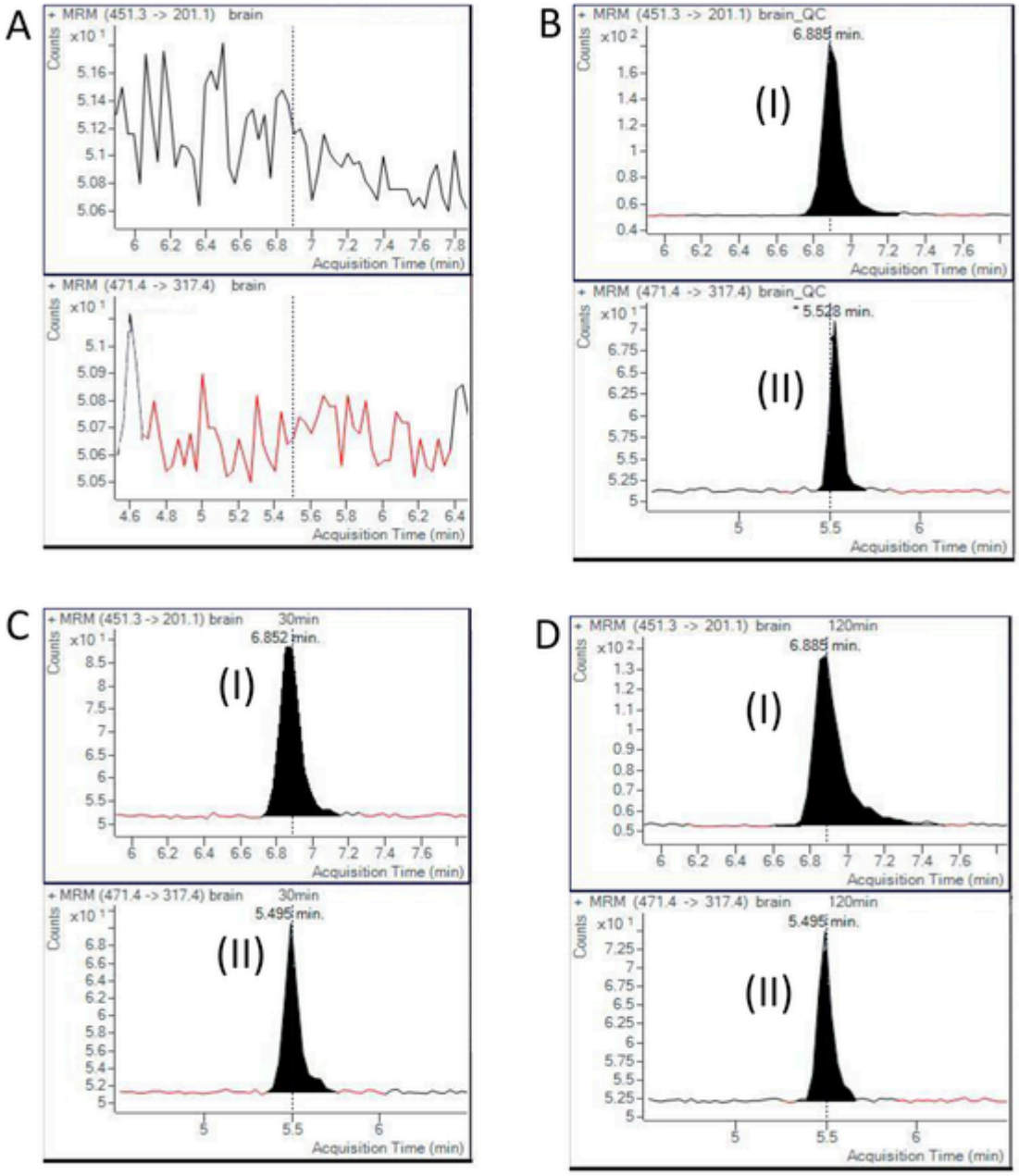

Fig. 2. Multiple reaction monitoring chromatograms of celastrol (I) and glycyrrhetinic acid (IS; II). (A) blank mouse brain; (B) blank mouse brain spiked with celastrol (50 pg/μL) and IS (20 pg/μL); (C) mouse brain sample 30 min after i.p. injection of celastrol (100 μg/kg BW); (D) mouse brain sample 120 min after i.p. injection of celastrol (100 μg/kg BW).

Table 2
Intra-day and inter-day precision and accuracy of celastrol in mouse brain samples.

Intra-day (n = 3)				Inter-day (n = 11)		
Spiked conc. [a] (pg/μL)	Concentration measured (pg/μL)	Precision (% RSD)	Accuracy (%)	Concentration measured (pg/μL)	Precision (% RSD)	Accuracy (%)
5	4.21 ± 0.16	3.8	84.2	4.65 ± 0.95	20.4	93.0
50	51.59 ± 3.89	7.7	103.2	52.4 ± 10.4	19.8	104.8

[a] 100 μL of standard solution, at given concentration, is spiked into about 50 mg of tissue extract.

mice to confirm the selectivity of our detection. As shown in Fig. 3A, no interference was observed in the representative chromatogram of the blank sample at the retention time of the analyte and internal standard. In contrast, the pooled hypothalamus sample from treated mice showed a distinct peak and thus a clear accumulation of celastrol in the hypothalamus (Fig. 3B). However, a signal to noise ratio of 7 for the celastrol peak did not allow an accurate quantification in the hypothalamus. We can nonetheless conclude from our qualitative data that celastrol reaches hypothalamic centers of feeding control. Future studies, built upon pooled hypothalamus samples and/or our method with

Table 3
Stability of celastrol spiked in mouse brain extracts ($n = 3$).

Stability conditions	Spiked conc. [a] (pg/μL)	Concentration measured (pg/μL)	Precision (% RSD)	Accuracy (%)
Short-term (10 °C, 6h autosampler)	5	4.22 ± 0.88	20.8	84.4
	50	46.08 ± 8.12	17.6	92.2
Mid-term (−20 °C for 3 days)	5	3.80 ± 0.45	11.2	76.0
	50	46.2 ± 10.4	22.5	92.4
Long-term (−80 °C for 2 weeks)	5	3.71 ± 0.26	7.0	74.2
	50	38.7 ± 1.8	4.7	77.3

[a] 100 μL of standard solution, at given concentration, is spiked into about 50 mg of tissue extract.

Table 4
Concentration of celastrol in mouse liver and brain at 30 min and 120 min post injection.

Organs	Time (min)	Concentration (pg/mg)
Liver [a]	30	32.60 ± 8.21
	120	40.52 ± 15.6
Brain [b]	30	4.70 ± 0.31
	120	16.22 ± 3.33

[a] Analysis performed with four animals per time point.
[b] Analysis performed with two animals per time points.

further improvements in the recovery efficiency and sensitivity, should help to clarify the exact concentration of bioactive celastrol reaching its target area in the hypothalamus, or elsewhere in the CNS.

4. Conclusions

An LC-MS method was developed for the quantification of celastrol in murine liver, brain and hypothalamus after the intraperitoneal administration of 100 μg/kg BW. We report levels of 32.6 ± 8.2 pg/mg celastrol in the liver and 8-fold lower levels in the brain of mice sacrificed 30 min post injection. One hundred and 20 min after the injection, hepatic celastrol levels remain stable but brain celastrol levels accumulate 4-fold to 16.2 ± 3.33 pg/mg. An earlier report using 40-times higher celastrol doses found a higher liver to brain ratio (Huang et al., 2012), which indicates the accumulation of high dose celastrol preferentially in the liver compared to other organs. However, a more complete assessment of the biodistribution, performed at different time points and with different concentrations and routes of administration, would be required to fully interrogate this behavior of celastrol. Overall, we report: (i) an analytical method suitable for multiple mouse organs that quantifies celastrol in tissues with notoriously high concentrations (liver) but also in tissues where concentrations are low (brain); (ii) considerably lower hepatic accumulation of low dose celastrol compared to earlier values reported for high dose treatment, thus suggesting a low hepatotoxicity risk for low dose celastrol treatment; (iii) celastrol can be found in the brain when administered as anti-obese drug; (iv) celastrol can be detected in the hypothalamus where it can reach its target cells and molecules.

Collectively, our findings on celastrol accumulation in the CNS and hypothalamus add to a growing body of literature that suggests celastrol as a hypothalamic leptin sensitizer, likely driven via non-competitive PTP1B and TCPTP inhibition (Kyriakou et al., 2018) and/or galanin (Fang et al., 2019) and IL1R1 signaling (Feng et al., 2019), that regulates our CNS control of feeding and body weight (Liu et al., 2015; Pfuhlmann et al., 2018).

Author statement

All authors have seen and approved the final version of the manuscript being submitted. They warrant that the article is the authors' original work, hasn't received prior publication and isn't under consideration for publication elsewhere. The authors declare that they have no known competing financial interests or personal relationships that could have appeared to influence the work reported in this paper. The authors declare no conflict of interest.

Declaration of competing interest

The authors declare no conflict of interest.

RECTED PROOF

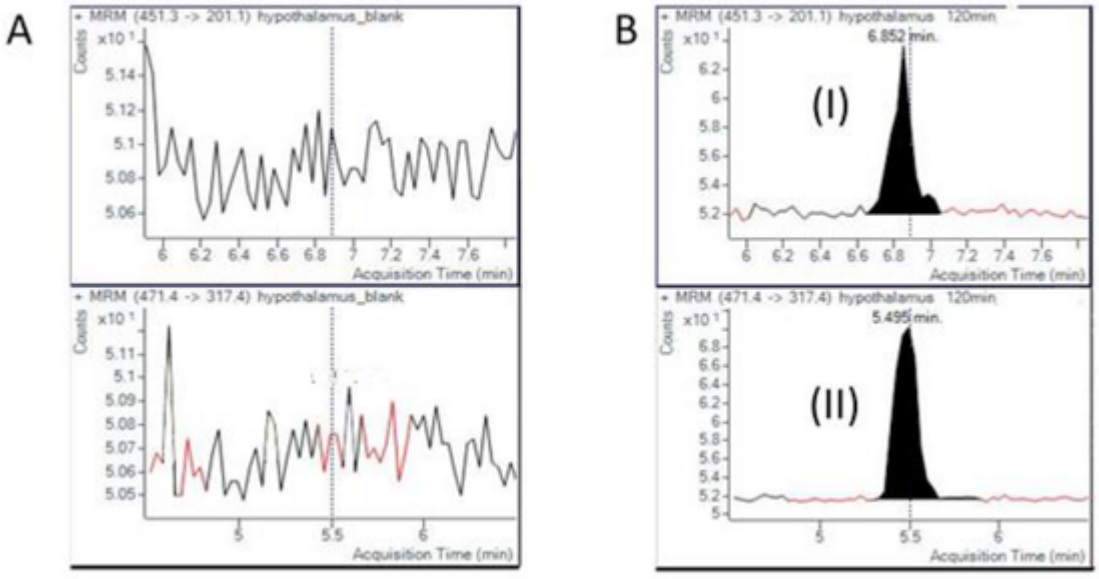

Fig. 3. Multiple reaction monitoring chromatograms of celastrol (I) and glycyrrhetinic acid (IS; II): (A) blank mouse hypothalamus; (B) sample pooled from 2 mouse hypothalami 120 min after i.p. injection of celastrol (100 μg/kg BW).

Acknowledgment

The authors would like to thank Agilent Technologies for supporting this research project. This work was supported in part by the Helmholtz Portfolio Program "Metabolic Dysfunction" (M.S.), and by an IMF Diabetes Portfolio grant (A.C.M., M.S.)

Appendix A. Supplementary data

Supplementary data to this article can be found online at https://doi.org/10.1016/j.neuint.2020.104713.

References

Allison, A C, Cacabelos, R, Lombardi, V R M, Alvarez, X A, Vigo, C, 2000. Central nervous system effects of celastrol, a potent antioxidant and antiinflammatory agent. CNS Drug Rev. 6, 45–62.

Allison, A C, Cacabelos, R, Lombardi, V R M, Alvarez, X A, Vigo, C, 2001. Celastrol, a potent antioxidant and anti-inflammatory drug, as a possible treatment for Alzheimer's disease. Prog. Neuro Psychopharmacol. Biol. Psychiatr. 25, 1341–1357.

Bajos, N, Wellings, K, Laborde, C, Moreau, C, Grp, C S F, 2010. Sexuality and obesity, a gender perspective: results from French national random probability survey of sexual behaviours. Br. Med. J. 340.

Bluher, M, 2019. Obesity: global epidemiology and pathogenesis. Nat. Rev. Endocrinol. 15, 288–298.

Camelio, A M, Johnson, T C, Siegel, D, 2015. Total synthesis of celastrol, development of a platform to access celastroid natural products. J. Am. Chem. Soc. 137, 11864–11867.

Choi, S K, Park, S, Jang, S, Cho, H H, Lee, S, You, S, Kim, S H, Moon, H S, 2016. Cascade regulation of PPAR gamma(2) and C/EBP alpha signaling pathways by celastrol impairs adipocyte differentiation and stimulates lipolysis in 3T3-L1 adipocytes. Metab. Clin. Exp. 65, 646–654.

Fang, P H, He, B, Yu, M, Shi, M Y, Zhu, Y, Zhang, Z W, Bo, P, 2019. Treatment with celastrol protects against obesity through suppression of galanin-induced fat intake and activation of PGC-1a/GLUT4 axis-mediated glucose consumption. Biochim. Biophys. Acta (BBA) - Mol. Basis Dis. 1865, 1341–1350.

Feng, X D, Guan, D X, Auen, T, Choi, J W, Hernandez, M A S, Lee, J, Chun, H, Faruk, F, Kaplun, E, Herbert, Z, Copps, K D, Ozcan, U, 2019. IL1R1 is required for celastrol's leptin-sensitization and antiobesity effects. Nat. Med. 25, 575.

Gordon, L P, Diaz, A, Soghomonian, C, Nucci-Sack, A T, Weiss, J M, Strickler, H D, Burk, R D, Schlecht, N F, Ochner, C N, 2016. Increased body mass index associated with increased risky sexual behaviors. J. Pediatr. Adolesc. Gynecol. 29, 42–47.

Guo, L, Luo, S, Du, Z W, Zhou, M L, Li, P W, Fu, Y, Sun, X, Huang, Y, Zhang, Z R, 2017. Targeted delivery of celastrol to mesangial cells is effective against mesangioproliferative glomerulonephritis. Nat. Commun. 8.

Hakim, F, Kheirandish-Gozal, L, Gozal, D, 2015. Obesity and altered sleep: a pathway to metabolic derangements in children? Semin. Pediatr. Neurol. 22, 77–85.

Hou, W, Liu, B, Xu, H, 2020. Celastrol: progresses in structure-modifications, structure-activity relationships, pharmacology and toxicology. Eur. J. Med. Chem. 189, 112081.

Huang, Y L, Zhou, D, Hang, T J, Wu, Z H, Liu, J G, Xu, Q A, Xie, X S, Zuo, J L, Wang, Z, Zhou, Y X, 2012. Preparation, characterization, and assessment of the antiglioma effects of liposomal celastrol. Anti Canc. Drugs 23, 515–524.

James, W P T, 2018. Obesity: a global public health challenge. Clin. Chem. 64, 24–29.

Kannaiyan, R, Shanmugam, M K, Sethi, G, 2011. Molecular targets of celastrol derived from Thunder of God Vine: potential role in the treatment of inflammatory disorders and cancer. Canc. Lett. 303, 9–20.

Kashyap, D, Sharma, A, Tuli, H S, Sak, K, Mukherjee, T, Bishayee, A, 2018. Molecular targets of celastrol in cancer: recent trends and advancements. Crit. Rev. Oncol.-Hematol. 128, 70–81.

Kelestimur, H, Canpolat, S, Kacar, E, Ozcan, M, 2017. Obesity and brain. Acta Physiol. 221 24-24.

Kim, D H, Shin, E K, Kim, Y H, Lee, B W, Jun, J G, Park, J H Y, Kim, J K, 2009. Suppression of inflammatory responses by celastrol, a quinone methide triterpenoid isolated from Celastrus regelii. Eur. J. Clin. Invest. 39, 819–827.

Kyriakou, E, Schmidt, S, Dodd, G T, Pfuhlmann, K, Simonds, S E, Lenhart, D, Geerlof, A, Schriever, S C, De Angelis, M, Schramm, K W, Plettenburg, O, Cowley, M A, Tiganis, T, Tschop, M H, Pfluger, P T, Sattler, M, Messias, A C, 2018. Celastrol promotes weight loss in diet-induced obesity by inhibiting the protein tyrosine phosphatases PTP1B and TCPTP in the hypothalamus. J. Med. Chem. 61, 11144–11157.

Liu, J L, Lee, J, Hernandez, M A S, Mazitschek, R, Ozcan, U, 2015. Treatment of obesity with celastrol. Cell 161, 999–1011.

Ma, X R, Xu, L Y, Alberobello, A T, Gavrilova, O, Bagattin, A, Skarulis, M, Liu, J, Finkel, T, Mueller, E, 2015. Celastrol protects against obesity and metabolic dysfunction through activation of a HSF1-PGC1 alpha transcriptional axis. Cell Metabol. 22, 695–708.

McElroy, S L, Kotwal, R, Malhotra, S, Nelson, E B, Keck, P E, Nemeroff, C B, 2004. Are mood disorders and obesity related? A review for the mental health professional. J. Clin. Psychiatr. 65, 634–651.

Mueller, K, Sacher, J, Arelin, K, Holiga, S, Kratzsch, J, Villringer, A, Schroeter, M, 2012. Overweight and obesity are associated with neuronal injury in the human cerebellum and hippocampus in young adults: a combined MRI, serum marker and gene expression study. Transl. Psychiatry 2.

Peng, B, Xu, L M, Cao, F F, Wei, T X, Yang, C X, Uzan, G, Zhang, D H, 2010. HSP90 inhibitor, celastrol, arrests human monocytic leukemia cell U937 at G0/G1 in thiol-containing agents reversible way. Mol. Canc. 9.

Pfuhlmann, K, Schriever, S C, Baumann, P, Kabra, D G, Harrison, L, Mazibuko-Mbeje, S E, Contreras, R E, Kyriakou, E, Simonds, S E, Tiganis, T, Cowley, M A, Woods, S C, Jastroch, M, Clemmensen, C, De Angelis, M, Schramm, K W, Sattler, M, Messias, A C, Tschop, M H, Pfluger, P T, 2018. Celastrol-induced weight loss is driven by hypophagia and independent from UCP1. Diabetes 67, 2456–2465.

Simon, S.L., Behn, C.D., Laikin, A., Kaar, J.L., Rahat, H., Cree-Green, M., Wright, K.P., Nadeau, K.J., Sleep & circadian health are associated with mood & behavior in adolescents with overweight/obesity. Behav. Sleep Med..

Sreeramulu, S, Gande, S L, Gobel, M, Schwalbe, H, 2009. Molecular mechanism of inhibition of the human protein complex hsp90-cdc37, a kinome chaperone-cochaperone, by triterpene celastrol. Angew. Chem. Int. Ed. 48, 5853–5855.

Trott, A, West, J D, Klaic, L, Westerheide, S D, Silverman, R B, Morimoto, R I, Morano, K A, 2008. Activation of heat shock and antioxidant responses by the natural product celastrol: transcriptional signatures of a thiol-targeted molecule. Mol. Biol. Cell 19, 1104–1112.

Wang, G, Xiao, Q, Wu, Y, Wei, Y J, Jing, Y, Cao, X R, Gong, Z N, 2019. Design and synthesis of novel celastrol derivative and its antitumor activity in hepatoma cells and antiangiogenic activity in zebrafish. J. Cell. Physiol. 234, 16431–16446.

Wang, H, Yang, Q Z, Dou, Q P, Yang, H J, 2018. Discovery of natural proteasome inhibitors as novel anticancer therapeutics: current status and perspectives. Curr. Protein Pept. Sci. 19, 358–367.

Wang, W W, Liu, K, Dong, H W, Liu, W H, 2008. High-performance liquid chromatography spectrometric analysis of tripterin in rat plasma. J. Chromatogr. B Anal. Technol. Biomed. Life Sci. 863, 163–166.

Xu, Q, Huang, M, Jin, M C, Ren, Q L, 2007. LC-APCI-MS-MS for the determination of celastrol in human whole blood. Chromatographia 66, 735–739.

Yan, G K, Zhang, H H, Wang, W, Li, Y, Mao, C H, Fang, M Q, Yi, X H, Zhang, J D, 2017. Investigation of the influence of glycyrrhizin on the pharmacokinetics of celastrol in rats using LC-MS and its potential mechanism. Xenobiotica 47, 607–613.

Zhang, J, Li, C Y, Xu, M J, Wu, T, Chu, J H, Liu, S J, Ju, W Z, 2012. Oral bioavailability and gender-related pharmacokinetics of celastrol following administration of pure celastrol and its related tablets in rats. J. Ethnopharmacol. 144, 195–200.

Zhang, Y L, Geng, C, Liu, X Y, Li, M X, Gao, M Y, Liu, X J, Fang, F D, Chang, Y S, 2017. Celastrol ameliorates liver metabolic damage caused by a high-fat diet through Sirt1. Mol. Metab. 6, 138–147.

UNCORRECTED PROOF